1.7 ON THE ENTRAINMENT LAW AT THE TOP OF THE CONVECTIVELY-DRIVEN ATMOSPHERIC BOUNDARY LAYER *

Charles Chemel †, Chantal Staquet and Jean-Pierre Chollet
Laboratoire des Ecoulements Géophysiques et Industriels, CNRS – UJF – INPG, Grenoble, France

ABSTRACT

We discuss the entrainment processes at the top of the convectively-driven boundary layer. The discussion is based on results from a high-resolution (256^3 grid points) large-eddy simulation initialized by a commonly used sounding of Day 33 of the Wangara experiment. We find that the mixed-layer turbulence precisely follows the Kolmogorov spectral law for the velocity field, whether two-dimensional (in horizontal planes) or one-dimensional spectra are computed. This behavior also holds for the frequency spectrum, when the Taylor's frozen turbulence hypothesis is used. As well, the fluctuating virtual potential temperature field follows the Corrsin-Oboukhov spectral law. The multiplicative constants of the power laws, inferred from the compensated spectra, are found to be in good agreement with previous measurements in the atmosphere. We next revisit the entrainment law at the mixed-layer top from two complementary Eulerian and Lagrangian approaches. The Lagrangian approach yields similar results to the eulerian one: the normalized entrainement velocity $w_e/w_\star$, where w_e and $w_\star$ are the entrainment and convective velocities, is found to vary as a function of the bulk Froude number squared at the interface with a multiplicative constant close to 1.2.

1. INTRODUCTION

The interfacial layer between the convectively-driven atmospheric boundary layer (CBL) and the free atmosphere is subjected to intense turbulent mixing, due to entrainment of air by convective motions. As a result of the entrainment processes, the interfacial layer raises (or the boundary layer deepens) at the entrainment velocity $w_e = d\overline{z_i}/dt$, with $\overline{z_i}$ being the horizontally-averaged mixed-layer depth. Fig. 1 from Chemel et al. (2006) is a visualization of the instantaneous interfacial layer using virtual potential temperature contours from a large-eddy simulation of the Day 33 of the Wangara experiment (Clarke et al. 1971). It shows that the interfacial layer is strongly turbulent and has a rich structure. Thus, the thickness of the interface has a high variability. Updrafts originating from the warm underlying ground surface strike the interfacial layer sharply (that leads to a folding of the interface) or erode the interface by a 'scouring' mechanism. The free atmosphere air above is then entrained into the mixed layer. These entrainment events are localized and the entrained air is mixed downward as the updrafts sink back into the mixed layer.

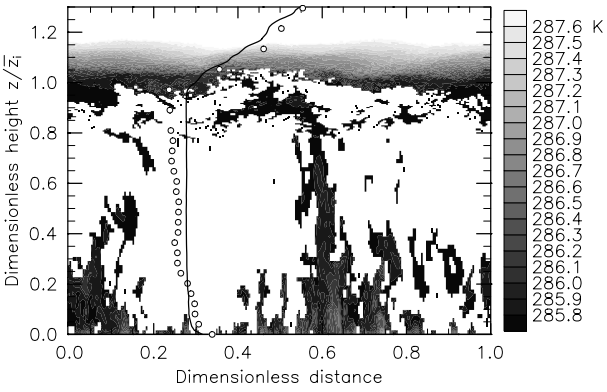

Figure 1: Visualization of the interfacial layer using resolved virtual potential temperature $\widetilde{\theta_v}$ contours in a (x, z) from a large-eddy simulation of the Day 33 of the Wangara experiment in a vertical plane (x, z) located in the vicinity of an updraft at 1500 EST. The distances along x and z are normalized by the domain length and the mixed-layer depth, respectively. Grayscale color table indicates $\widetilde{\theta_v}$ variations at the interface (lower and higher $\widetilde{\theta_v}$ appear white). Both $\widetilde{\theta_v}$ profiles measured during the Wangara experiment ($\circ$) and computed from the LES outputs as a horizontally-averaged profile over the computational domain (—) are also included for comparison purpose. From Chemel et al. (2006).

*This short paper is based on Chemel et al. (2006), which has been submitted to *J. Atm. Sci.*

†*Corresponding author address:* Dr. Charles Chemel, Laboratoire des Ecoulements Géophysiques et Industriels, CNRS – UJF – INPG, BP 53, 38041 Grenoble, Cedex 9, France; e-mail: Charles.Chemel@hmg.inpg.fr.

As pointed out *f.i.* by Otte and Wyngaard (2001), the modeling of the entrainment process is an essential issue for both oceanic and atmospheric applications. Thus, several entrainment law formulations have been derived out to date, starting from the 'zero-order' jump model of turbulent entrainment by Ball (1960) and Lilly (1968). A thorough review of more general formulations in the shear-free CBL can be found in Fedorovich et al. (2004).

From an experimental point of view, the entrainment processes across a density interface has extensively been studied. Hopfinger (1987) and Fernando (1991) gave a review for an interfacial layer that is destabilized by grid turbulence. The entrainment process is classically discussed as a function of a bulk Richardson number at the interface, defined as

$$\mathrm{Ri}_B = g\ \beta\ \Delta\theta_v\ \overline{z_i}/w_\star^2, \tag{1}$$

where $\Delta\theta_v$ is the horizontally-averaged virtual potential temperature jump across the interface and $w_\star$ is the convective velocity, g the gravitational acceleration and β the coefficient of thermal expansion. Hereafter, the overbar $\overline{\square}$ stands for a spatial average in a horizontal plane. The convective velocity within the mixed layer is expressed as

$$w_\star = \left[g\ \beta\ \left(\overline{w'\theta'_v}\right)_s\ \overline{z_i}\right]^{1/3}, \tag{2}$$

where $\left(\overline{w'\theta'_v}\right)_s$ is the average heat flux just above the ground surface. When entrainment results from grid generated turbulence, the dimensionless entrainment rate $w_e/w_\star$ was found to scale like Ri_B^{-n}, where n is in the range $1-2$ depending upon the values of the Prandtl and Richardson numbers. In the convection tank experiment of Deardorff et al. (1980), the dimensionless entrainment velocity was found to vary as

$$w_e/w_\star = A\ \mathrm{Ri}_B^{-1}, \tag{3}$$

where $A = 0.25$. As noted by Deardorff et al. (1980), the entrainement law (3) immediately follows from the 'zero-order model' with an entrainement ratio equal to 0.25. Deardorff et al. (1980) claimed that their data could also be fitted by the law $w_e/w_\star = 1.1\ \mathrm{Ri}_B^{-3/2}$, so that there seemed to be no clear dependence on Ri_B.

The entrainment processes have also been investigated in several large-eddy simulations (LESs). The entrainment law (3) is generally retrieved for the convectively-driven boundary layer (*e.g.* Sullivan et al. 1998; Chemel et al. 2006). Nevertheless different LES investigations show a scatter of about 30 % in the value of the dimensionless parameter A (Stevens and Lenschow 2001). In this study, we present our results from a high-resolution (256^3 grid points) large-eddy simulation of the convectively-driven (shear-free) boundary layer initialized by a commonly used sounding of Day 33 of the Wangara experiment (Clarke et al. 1971). This 'realistic' initialization enables us to validate further our numerical results. The objectives of the paper are *(i)* to investigate the mixed-layer dynamics, which forces the interfacial layer, from a statistical point of view, and *(ii)* to revisit and discuss the Ri_B^{-1} entrainment law (3), using an Eulerian approach (*i.e.* the LES) and a Lagrangian approach (*i.e.* a Lagrangian stochastic model coupled with the LES).

The numerical experiments presented in this paper were conducted with the Advanced Regional Prediction System (ARPS), a non-hydrostatic, compressible LES code devoted to meso-scale as well as small-scale atmospheric flows. Xue et al. (2000; 2001) gave an extensive description of the model formulation and applications. A lagrangian particle dispersion model has also been implemented in the ARPS code to track a large number of particle positions. A detailed description of the model and setup of the LES can be found in Chemel et al. (2006).

The outline of the short paper is then as follows. In § 2.1, we investigate the mixed layer to characterize the mechanisms responsible for the destabilization of the interfacial layer. We analyze the mixed-layer dynamics both from a statistical point of view, by computing 1D and 2D spatial as well as temporal spectra. In § 2.2, the entrainment rate formulation is discussed based on LES and particle dispersion outputs, and expressed as a function of a Froude number at the interface. Finally, concluding remarks are given in § 3.

2. RESULTS & DISCUSSION

2.1 *Mixed-layer statistics*

Since the mixed layer is homogeneous (in a statistical sense) in a horizontal plane, it is natural to consider horizontal 2D Fourier transforms. The expression of the 2D kinetic energy spectrum in the inertial range (between the integral scale and the dissipative scale) is given by (Chemel et al. 2006)

$$E_\perp\left(k_\perp, t\right) = C_2\ \overline{\epsilon}^{2/3}\ k_\perp^{-5/3}, \tag{4}$$

where ϵ is the turbulent kinetic energy dissipation rate and $k_\perp^2 = k_x^2 + k_y^2$. The constant C_2 is expressed as a function of the Kolmogorov constant C_K, namely $C_2 = C_K\ \sqrt{\pi}/2\ \mathcal{F}_\Gamma\left(4/3\right)/\mathcal{F}_\Gamma\left(11/6\right)$, with $\mathcal{F}_\Gamma$ being the Gamma function. Measurements

in the atmosphere suggested that C_K is in the order of 1.5 (Champagne et al. 1977). Hence, for $C_K = 1.5$, this yields $C_2 \approx 1.26$. The integral scale was computed as $\ell_i = 2\pi/k_i = \widetilde{u_{rms}}^3/\overline{\epsilon}$, where $\widetilde{u_{rms}}$ is the root-mean-square of the horizontal velocity components. As for the dissipative scale, it is calculated as $\ell_v = 2\pi/k_v = \left(\overline{\nu_t}^3/\overline{\epsilon}\right)^{1/4}$, where ν_t is the turbulent viscosity.

In Fig. 2a, $E_\perp\left(k_\perp\right)$ averaged over the range $0.4 < z/\overline{z_i} < 0.6$ at 1500 EST is displayed versus $k_\perp$, for two different resolutions. The computed integral scale is close to 1900 m, which roughly corresponds to the typical size of the convective cells (*e.g.* Schmidt and Schumann 1989; Chemel et al. 2006). In the present LES the dissipative scale ℓ_v is in the order of 5 m. The Kolmogorov law is observed over almost a decade in the inertial range for the 256^3 resolution run. As a comparison, the kinetic energy spectrum computed with a 128^3 resolution is superimposed in Fig. 2a. It exhibits only a half decade in the inertial range. To compare rigorously the computed spectrum with inertial-range theory, the compensated spectrum $E_\perp\ \overline{\epsilon}^{-2/3}\ k_\perp^{5/3} = C_2$ is displayed as a function of $k_\perp$ in the subplot of Fig. 2a. In the inertial range, C_2 remarkably averages about the predicted value of 1.26.

If the CBL is well-mixed, the virtual potential temperature $\widetilde{\theta_v}$ should behave as a passive scalar. We assume thereafter that the wavenumbers characteristic of the peaks of both kinetic energy and virtual potential temperature spectra are identical. This is a reasonable hypothesis since these wavenumbers are both imposed by the large convective motions. In the inertial-convective range (namely $k_i \ll k_\perp \ll k_d$, where $k_d = 2\pi/\ell_d$ with $\ell_d = \left(\overline{\kappa_t}^3/\overline{\epsilon}\right)^{1/4}$ for $\mathrm{Pr}_t < 1$, which is the case here), the 2D spectrum of virtual potential temperature variance follows the Corrsin-Oboukhov law (Chemel et al. 2006)

$$E_{\theta,\perp}\left(k_\perp, t\right) = C_{CO,2}\ \overline{\epsilon_\theta}\ \overline{\epsilon}^{-1/3}\ k_\perp^{-5/3}, \qquad (5)$$

with $\overline{\epsilon_\theta}$ being the dissipation rate of one half the average virtual potential temperature variance, which is given by $\overline{\epsilon_\theta} = \kappa_s\ \overline{\left(\partial_i \widetilde{\theta_v}\right)^2}$, where κ_s is the subgrid-scale thermal diffusivity. A derivation analogous to that leading to the expression of C_2 gives $C_{CO,2} = C_{CO}\ \sqrt{\pi}/2\ \mathcal{F}_\Gamma\left(4/3\right)/\mathcal{F}_\Gamma\left(11/6\right)$, where C_{CO} is the Corrsin-Oboukhov constant. Using measurements in the atmosphere, Champagne et al. (1977) found $C_{CO} \approx 0.64$. For $C_{CO} = 0.64$, this yields $C_2 \approx 0.54$.

In Fig. 2b we compare the virtual potential temperature variance spectrum $E_{\theta,\perp}\left(k_\perp\right)$ derived from our LES outputs with the theoretical prediction in relation (5). Our results agree well with the Corrsin-Oboukhov spectrum over almost a decade. Dividing the spectra by $\epsilon_\theta\ \epsilon^{-1/3}\ k_\perp^{-5/3}$ gives the value of $C_{CO,2}$, which is displayed versus $k_\perp$ in the subplot of Fig. 2b. The agreement of $C_{CO,2}$ with the theoretical prediction of 0.54 is correct over the range of wavenumbers for which $E_{\theta,\perp}$ closely follows a $k_\perp^{-5/3}$ power law, that is for the smallest scales of the inertial range. In overall, we may say that the passive scalar assumption for $\widetilde{\theta_v}$ is quite justified.

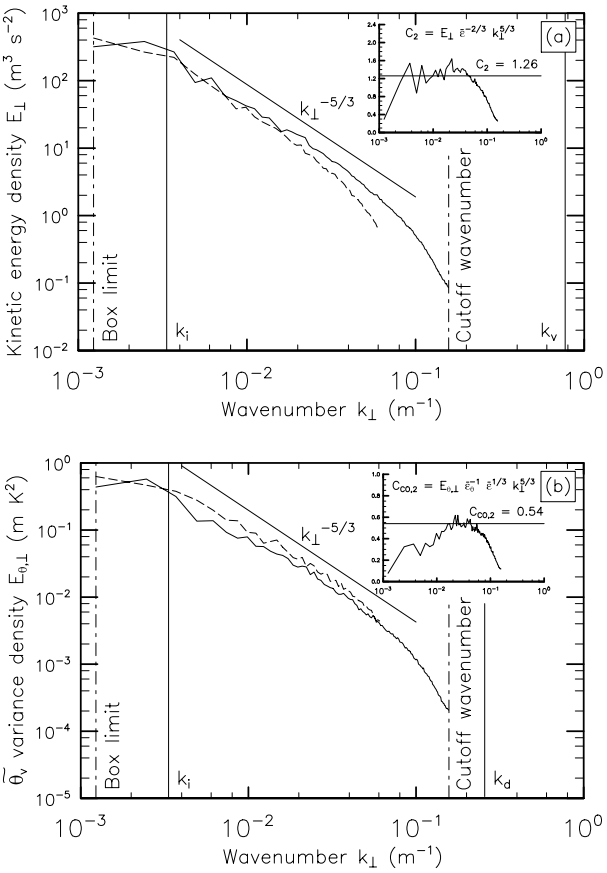

Figure 2: **(a)** 2D kinetic energy spectrum $E_\perp\left(k_\perp\right)$ at 1500 EST computed for the 256^3 resolution run (—) and averaged over the range $0.4 < z/\overline{z_i} < 0.6$. The subplot displays computed constant C_2 in relation (4) as a function of $k_\perp$. The spectrum computed for a 128^3 resolution run (- - -) is superimposed as a comparison. **(b)** As in (a), but for 2D virtual potential temperature variance spectrum $E_{\theta,\perp}\left(k_\perp\right)$ and computed constant $C_{CO,2}$ in relation (5). From Chemel et al. (2006).

Let us examine the assumption of local isotropy in the horizontal plane. Fig. 3a displays the 1D longitudinal spectra of $\widetilde{u}$ and $\widetilde{v}$ as a function of k_x and k_y, respectively, for two different resolutions, averaged over the range $0.4 < z/\overline{z_i} < 0.6$ at 1500 EST. The spectra along k_x and k_y are nearly the same,

which is consistent with local isotropy. From a theoretical point of view, if turbulence is homogeneous and isotropic, these spectra should behave as

$$E_{ii}\left(k_i,t\right) = C_1\ \overline{\epsilon}^{2/3}\ k_i^{-5/3}, \tag{6}$$

with k_i being k_x or k_y, and $C_1 = (18/55)\ C_K \approx 0.49$ for $C_K = 1.5$ (*e.g.* Champagne et al. 1977; Moeng and Wyngaard 1988). The numerically computed spectrum of $\widetilde{u}$ normalized by $\overline{\epsilon}^{-2/3}\ k_x^{5/3}$ is displayed versus k_x in the subplot of Fig. 3a. The value of C_1 thus obtained agrees well with the theoretical prediction of 0.49 for the smallest scales of the inertial range.

Since the large-scale flow within the mixed layer consists of convective cells, the scales contributing to the inertial range may be assumed to be advected by those cells. Thence, the Taylor's (1938) frozen turbulence hypothesis may be assumed to hold. This reasoning also requires that the magnitude of the velocity fluctuations be much smaller than the convective velocity. Under these assumptions, a $f^{-5/3}$ power law, with f being the frequency, is expected in the inertial range for scalar quantities as well as for velocity components. The frequency spectrum of $\widetilde{u}$, $S_u\left(f\right)$, computed from 1200 EST to 1500 EST at $z = 500$ m in the center of the (x,y) plane, is displayed versus f in Fig. 3b: a $-5/3$ inertial range is obtained over almost a decade. The overturning time scale associated with the integral scale may be estimated by $\tau_i = \tau_{\text{eddy}}\left(\ell_i\right) = \ell_i/\widetilde{u_{rms}}$, and is in the order of 15 min. This is indeed the typical time period for air to circulate between the ground surface and the mixed-layer top, *i.e.* roughly $\overline{z_i}/w_\star$, as we checked it.

Since the Taylor's hypothesis is assumed to hold, temporal spectra gathered in this way can be converted to 1D spatial spectra by substituting the frequency f for $k_x\left|\widetilde{\mathbf{u}}\right|$. The 1D spatial spectrum thus obtained is superimposed upon E_{ii} in Fig. 3a: both spectra remarkably coincide over the inertial range, which demonstrates the reliability of the Taylor's hypothesis within the mixed layer.

2.2 *Entrainment rate formulation*

In this section, the focus is directed onto the interfacial layer, where turbulence is damped by buoyancy forces. As stressed by Chemel and Staquet (2006), the Froude number Fr_B of the interfacial layer is the most appropriate dynamical parameter to characterize the interface in the convectively-driven boundary layer. This parameter is defined as the ratio of the characteristic frequency $w_\star/\overline{z_i}$ of the turbulent motions, which destabilize the interface, to

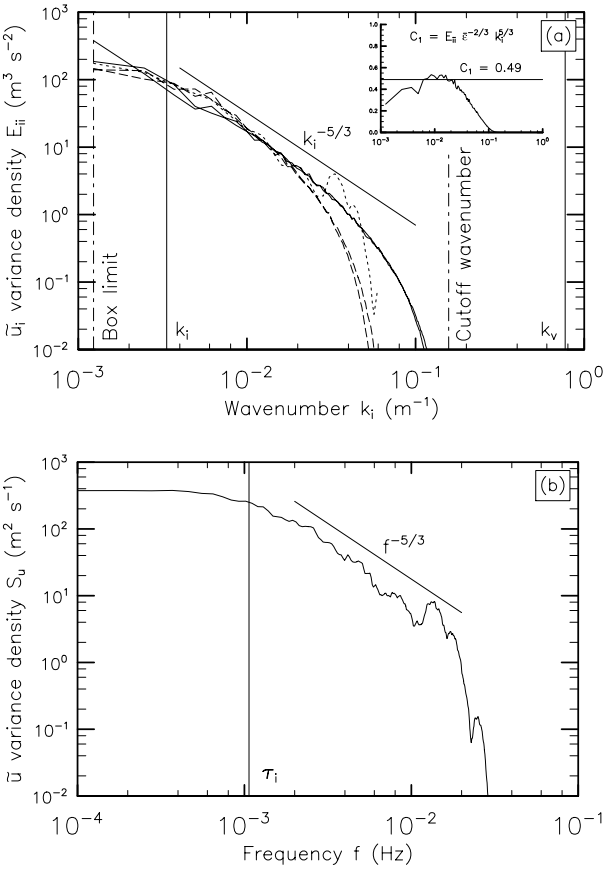

Figure 3: **(a)** 1D longitudinal velocity spectra $E_{ii}\left(k_i\right)$ of $\widetilde{u}$ and $\widetilde{v}$ at $t =$ 1500 EST computed for the 256^3 resolution run (—) and averaged over the range $0.4 < z/\overline{z_i} < 0.6$. The subplot displays computed constant C_1 in relation (6) averaged over both $\widetilde{u}$ and $\widetilde{v}$ spectra as a function of k_i. The spectra computed for a 128^3 resolution run (- - -) are superimposed as a comparison. The dotted line ($\cdot\ \cdot\ \cdot$) represents the spectrum of u deduced from the frequency velocity spectrum $S_u\left(f\right)$ of $\widetilde{u}$, displayed in plot **(b)** and computed for the 256^3 resolution run, from 1200 EST to 1500 EST at $z = 500$ m in the center of the (x,y) plane. From Chemel et al. (2006).

the buoyancy frequency $N = \sqrt{g\ \beta\ \partial_3\widetilde{\theta_v}}$ at the interface, which characterizes it stability. Hence,

$$\mathrm{Fr}_B = w_\star/\left(N\ \overline{z_i}\right). \tag{7}$$

One may note that Fr_B^2 is the inverse of the Ri_N number introduced by Fedorovich et al. (2004). With N aproximated by $\sqrt{g\ \beta\ \Delta\theta_v/\Delta h}$, the parameters Fr_B and Ri_B are related by $\mathrm{Ri}_B = \left(\Delta h/\overline{z_i}\right)\mathrm{Fr}_B^{-2}$, where Δh is the horizontally-averaged mixed-layer thickness. The entrainment law (3) then becomes

$$w_e/w_\star = B\ \mathrm{Fr}_B^2, \tag{8}$$

where $B = A\,(\overline{z_i}/\Delta h)$. The value of B appears to be a constant of about 1.2 in the regime of equilibrium entrainment (Fedorovich et al. 2004; Chemel and Staquet 2006).

In the following, we check upon the reliability of the latter entrainment law from our LES results using both Eulerian and Lagrangian approaches.

Characteristics of the simulated interfacial layer are given in Chemel et al. (2006) (their Table 1). In respect to the Eulerian approach, the horizontally-averaged entrainment velocity, namely

$$w_e = d_t \overline{z_i}, \tag{9}$$

is directly computed from the time derivative of $\overline{z_i}$ using a centered difference scheme.

A different approach using particle dispersion is proposed to retrieve the entrainment velocity w_e. Using first-order closure the heat flux is classically expressed as a function of the mean vertical gradient of virtual potential temperature, namely

$$-\overline{w'\theta'_v} = \kappa_t\, \partial_3 \overline{\widetilde{\theta}_v}. \tag{10}$$

Using the 'first-order' jump model framework proposed by Betts (1974), the heat flux across the interfacial layer $\left(\overline{w'\theta'_v}\right)_i$ is related to the entrainment velocity by

$$-\left(\overline{w'\theta'_v}\right)_i = w_e\, \Delta\theta_v - \delta h\, \partial_t \overline{\widetilde{\theta}_v}^{1,2}, \tag{11}$$

where $\delta h = \overline{z_2} - \overline{z_1}$ is the difference between the vertical position $\overline{z_2}$ where the heat flux first goes to zero above $\overline{z_i}$ and the vertical position $\overline{z_1}$ of the minimum heat flux, and $\overline{\widetilde{\theta}_v}^{1,2} = \left[\overline{\widetilde{\theta}_v}\,(z_1) + \overline{\widetilde{\theta}_v}\,(z_2)\right]/2$. In the limit of infinitely small thickness of the interfacial layer, *i.e.* $\delta h = 0$, relation (11) simply reduces to the 'zero-order' jump condition derived by Lilly (1968). Assuming again that $\Delta\theta_v/\Delta h$ is a good approximation of $\partial_3\widetilde{\theta_v}$ within the interfacial layer, relations (10) and (11) together yield

$$w_e = \kappa_t/\Delta h + \delta h\, \partial_t \overline{\widetilde{\theta}_v}^{1,2}/\Delta\theta_v. \tag{12}$$

The turbulent thermal diffusivity κ_t can be evaluated directly from the dispersion of fluid particles. By 'fluid particles', we mean non buoyant particles simply advected by the velocity field. Let $(\delta z)_{ms}\,(t)$ be the mean square vertical displacement of fluid particles at time t for a given release. It is written as

$$(\delta z)_{ms}\,(t) = (1/N_p) \sum_{n=1}^{N_p} \left[z_n\,(t) - z_G\,(t)\right]^2, \tag{13}$$

where N_p is the number of particles of the release, $z_n\,(t)$ is the vertical position of the particle n and $z_G\,(t)$ the vertical position of the center of gravity of the particle cloud at time t. If the turbulence is locally homogeneous and stationary, and for $t \geq 2\,\mathcal{T}_L$, with $\mathcal{T}_L$ being the Lagrangian time scale of the turbulence, κ_t can be inferred from the growth rate of $(\delta z)_{ms}$ (Taylor 1921; Hunt 1985, for a review), namely

$$d_t\,(\delta z)_{ms} = 2\,\kappa_t. \tag{14}$$

Since the interfacial layer is continuously forced by the quasi-stationary convective cells, the turbulence within this layer may be assumed stationary as well. For stationary and homogeneous turbulence, the Lagrangian time scale is in the same order of magnitude as the Eulerian time scale $\mathcal{T}_E$ [for isotropic turbulence, the ratio $\mathcal{T}_L/\mathcal{T}_E$ is close to 0.8 (Yeung 2002)]. This result also holds in the presence of a stable stratification (Hunt 1985) . In the present case $\mathcal{T}_E = \ell_b/\sigma_w$, where σ_w is the standard deviation of the fluctuating vertical velocity (*e.g.* Hopfinger 1987). From Otte and Wyngaard (2001), $\ell_b \approx 24$ m and $\sigma_w \approx 0.5$ m s^{-1} for conditions analogous to our LES (their cases 19 to 22), so that $\mathcal{T}_E \approx 48$ s implying that $2\,\mathcal{T}_L$ is in the order of 1 min.

Particles were carefully released within the bulk of the interfacial layer (approximately between $z - \overline{z_i} = \pm 100$ m) in a region centered approximately on the horizontal plane. Nevertheless some of the particles were released below and above the interfacial layer since its thickness varies over a wide range within the simulated domain. The releases were made at 4 equally-spaced times from 1155 EST to 1325 EST over 10-min periods and resulted in a total of 57500 particles per release. These release times were chosen because they correspond to a nearly constant ground surface heat flux. A quasi-linear growth occurs after about 1 min (not shown) whose growth rate may be interpreted as $2\,\kappa_t$. Values for κ_t between 2.94 and 3.83 m^2 s^{-1} were obtained depending upon the time of the release. κ_t varies with time since the interfacial-layer properties also vary with time.

The resulting Ri_B^{-1} and Fr_B^2 dependences of the parameters A and B in relations (3) and (8), respectively, with w_e values computed by relation (12), are shown in Fig. 4. The results are compared with those obtained when w_e is computed by relation (9), as well as with the convection tank measurements of Deardorff et al. (1980) over the region of common Ri_B^{-1} or equivalently Fr_B^2. A good agreement is found, with relative differences being lower than 10 % on average. This emphasizes that the particle dispersion approach is well adapted to derive

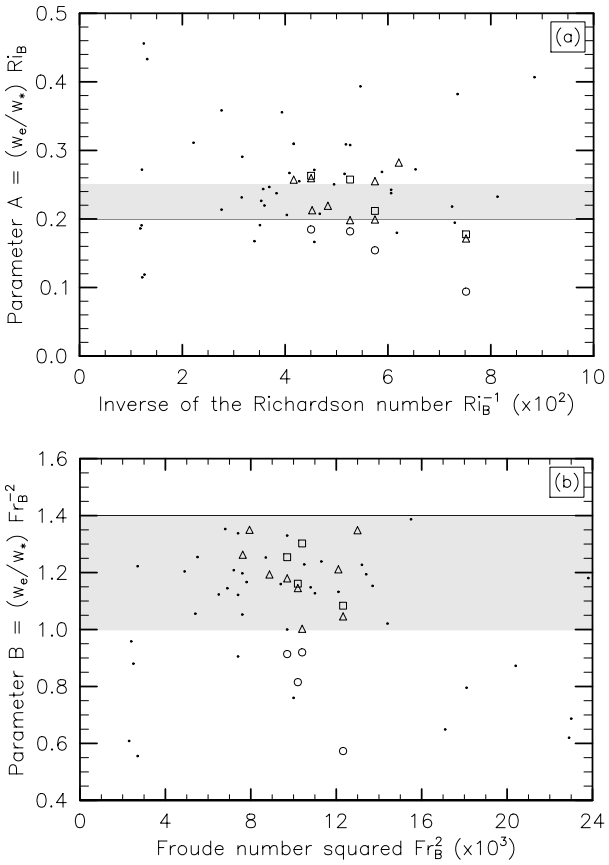

Figure 4: Dimensionless parameters: **(a)** $A = (w_e/w_\star)\,\mathrm{Ri}_B$ in relation (3) and **(b)** $B = (w_e/w_\star)\,\mathrm{Fr}_B^{-2}$ in relation (8). In each frame, the entrainment velocity w_e is computed by three different methods: the Eulerian approach as triangles [$\triangle$, relation (9)], the Lagrangian approach as squares [$\square$, relation (12)], and a simplified model in the Lagrangian approach, with w_e being computed as $\kappa_t/\Delta h$, as circles ($\circ$). The convection tank measurements of Deardorff et al. (1980) are also indicated as black dots ($\cdot$). The filled area represents: **(a)** A in the range $0.18 - 0.27$ and **(b)** B in the range $1.0 - 1.4$. From Chemel et al. (2006).

the properties of the interfacial layer. As a comparison, the values computed from a simplified model in the Lagrangian approach (namely, w_e computed as $\kappa_t/\Delta h$) are superimposed in Fig. 4. The magnitude of the term $\delta h\ \partial_t \overline{\widetilde{\theta_v}}^{1,2}/\Delta\theta_v$ in relation (12) is found to be not negligible compared with $\kappa_t/\Delta h$ in the range of Ri_B values considered in our LES. The former term indeed contribute to about $30 - 35$ % of the total entrainment velocity when Ri_B is strong enough (approximately larger than 15 according to our data). At low Ri_B, this term counts for more than 45 %. Our finding are consistent with the LES results of Sullivan et al. (1998).

3. CONCLUDING REMARKS

The entrainment processes at the top of the CBL were reexamined using data from high-resolution (256^3 grid points) LES. A detailed statistical analysis of the mixed-layer fields was performed. We found that the turbulence precisely follows the Kolmogorov spectral law for the velocity field, with a multiplicative constant in good agreement with previous measurements in the atmosphere, whether 2D (in horizontal planes) or 1D spectra are computed. This behavior also holds for the frequency spectrum, when the Taylor's frozen turbulence hypothesis is used. Hence, the turbulence within the mixed layer may be assumed to be locally homogeneous and isotropic. As well, the fluctuating virtual potential temperature field was found to follow the Corrsin-Oboukhov spectral law, both in power law and level. This is consistent with this field behaving as a passive scalar in the mixed layer.

The normalized entrainment velocity was found to vary as $w_e/w_\star = B\ \mathrm{Fr}_B^2$, with a multiplicative constant B of about 1.2. The scatter of our data points out the difficulties to estimate the boundaries of the interfacial-layer and consequently the values of $\Delta\theta_v$ and Δh. Nonetheless, the ratio of the interfacial-layer thickness to the convective mixed-layer depth in the limit of strong stratification was found to be in the order of 0.2, consistently with the convection tank measurements of Deardorff et al. (1980) when Ri_B is high enough.

A particle dispersion approach using LES coupled with a Lagrangian stochastic model was used to compute the entrainment velocity from relation (12). The derived values were in rather good agreement with those computed directly from $d_t\overline{z_i}$. Relative differences were found to be lower than 10 % on average. The 'first-order' jump model was found to work well. We find that the first order correction contributes to at least 30 % to the value of w_e. Still, the Lagrangian approach provides a very simple and useful expression for the entrainment velocity (namely, $w_e = \kappa_t/\Delta h$), from which a preliminary good estimate can be obtained in a straightforward manner. These results may have applications for remote sensing of the mixed-layer top.

Acknowledgements. All the major computations were realized with the *Institut du Développement et des Ressources en Informatique Scientifique* (IDRIS) computing resources. The authors thank I. Vinkovic, C. Aguirre and S. Simoëns for providing us with a part of the Lagrangian stochastic model and for helpful discussions.

REFERENCES

Ball, F. K., 1960: Control of inversion height by surface heating. *Quart. J. Roy. Met. Soc.*, **86**, 483–494.

Betts, A. K., 1974: Reply to comment on the paper 'non-precipitating cumulus convection and its parameterization'. *Quart. J. Roy. Met. Soc.*, **100**, 469–471.

Champagne, F. H., C. A. Friehe, J. C. LaRue, and J. C. Wyngaard, 1977: Flux measurements, flux estimation techniques, and fine-scale turbulence measurements in the unstable surface layer over land. *J. Atm. Sci.*, **34**, 515–530.

Chemel, C. and C. Staquet, 2006: On the entrainment law at the top of the convective boundary layer, submitted to *Quart. J. Roy. Met. Soc.*

Chemel, C., C. Staquet, and J.-P. Chollet, 2006: Entrainment processes at the top of the convectively-driven boundary layer from high-resolution large-eddy simulation, submitted to *J. Atm. Sci.*

Clarke, R. H., A. J. Dyer, R. R. Brook, D. G. Reid, and A. J. Troup, 1971: The Wangara experiment: Boundary layer data. Tech. Paper 19, CSIRO Atmospheric Research, Aspendale, Australia, 362 pp.

Deardorff, J. W., G. E. Willis, and B. H. Stockton, 1980: Laboratory studies of the entrainment zone of a convectively mixed layer. *J. Fluid Mech.*, **100**, 41–64.

Fedorovich, E., R. Conzemius, and D. Mironov, 2004: Convective entrainment into a shear-free, linearly stratified atmosphere: bulk models reevaluated through large eddy simulations. *J. Atm. Sci.*, **61**, 281–295.

Fernando, H. J. S., 1991: Turbulent mixing in stratified fluids. *Ann. Rev. Fluid Mech.*, **23**, 455–493.

Hopfinger, E. J., 1987: Turbulence in stratified fluids: a review. *J. Geophys. Res.*, **C92**, 5287–5303.

Hunt, J. C. R., 1985: Diffusion in the stably stratified atmospheric boundary layer. *J. Appl. Meteor.*, **24**, 1187–1195.

Lilly, D. K., 1968: Models of cloud-topped mixed layers under a strong inversion. *Quart. J. Roy. Met. Soc.*, **94**, 292–309.

Moeng, C.-H. and J. C. Wyngaard, 1988: Spectral analysis of large-eddy simulations of the convective boundary layer. *J. Atm. Sci.*, **45**, 3573–3587.

Otte, M. J. and J. C. Wyngaard, 2001: Stably stratified interfacial-layer turbulence from large-eddy simulation. *J. Atm. Sci.*, **58**, 3424–3442.

Schmidt, H. and U. Schumann, 1989: Coherent structure of the convective boundary layer derived from large-eddy simulations. *J. Fluid Mech.*, **200**, 511–562.

Stevens, B. and D. H. Lenschow, 2001: Observations, experiments, and large eddy simulation. *Bull. Am. Met. Soc.*, **82**, 283–294.

Sullivan, P. P., C.-H. Moeng, B. Stevens, D. H. Lenschow, and S. D. Mayor, 1998: Structure of the entrainment zone capping the convective atmospheric boundary layer. *J. Atm. Sci.*, **55**, 3042–3064.

Taylor, G. I., 1921: Diffusion by continuous movements. *Proc. London Math. Soc.*, **20**, 196–212.

— 1938: The spectrum of turbulence. *Proc. Roy. Soc. London*, **A164**, 476–490.

Xue, M., K. K. Droegemeier, and V. Wong, 2000: The Advanced Regional Prediction System (ARPS) – a multi-scale non hydrostatic atmospheric simulation and prediction model. Part I: Model dynamics and verification. *Met. Atm. Phys.*, **75**, 161–193.

Xue, M., K. K. Droegemeier, V. Wong, A. Shapiro, K. Brewster, F. Carr, D. Weber, Y. Liu, and D. Wang, 2001: The Advanced Regional Prediction System (ARPS) – a multi-scale non hydrostatic atmospheric simulation and prediction tool. Part II: Model physics and applications. *Met. Atm. Phys.*, **76**, 143–165.

Yeung, P. K., 2002: Lagrangian investigations of turbulence. *Ann. Rev. Fluid Mech.*, **34**, 115–142.